J Syst Sci Complex (2024) 37(5): 1956–1977

Vision-Based Adaptive Prescribed-Time Control of UAV for Uncooperative Target Tracking with Performance Constraint*

SHE Xuehua · MA Hui · REN Hongru · LI Hongyi

DOI: 10.1007/s11424-024-3443-2
Received: 19 October 2023 / Revised: 9 January 2024

Abstract This paper discusses the uncooperative target tracking control problem for the unmanned aerial vehicle (UAV) under the performance constraint and scaled relative velocity constraint, in which the states of the uncooperative target can only be estimated through a vision sensor. Considering the limited detection range, a prescribed performance function is designed to ensure the transient and steady-state performances of the tracking system. Meanwhile, the scaled relative velocity constraint in the dynamic phase is taken into account, and a time-varying nonlinear transformation is used to solve the constraint problem, which not only overcomes the feasibility condition but also fails to violate the constraint boundaries. Finally, the practically prescribed-time stability technique is incorporated into the controller design procedure to guarantee that all signals within the closed-loop system are bounded. It is proved that the UAV can follow the uncooperative target at the desired relative position within a prescribed time, thereby improving the applicability of the vision-based tracking approach. Simulation results have been presented to prove the validity of the proposed control strategy.

Keywords Nonlinear transformation, performance constraint, prescribed-time tracking, uncooperative target, vision-based measurement.

SHE Xuehua
School of Automation and the Guangdong Provincial Key Laboratory of Intelligent Decision and Cooperative Control, Guangdong University of Technology, Guangzhou 510006, *China.* Email: shexuehua2021@163.com.
MA Hui (Corresponding author)
School of Mathematics and Statistics, Guangdong University of Technology, Guangzhou 510006, *China.*
Email: huima2016@163.com.
REN Hongru
School of Automation and the Guangdong Provincial Key Laboratory of Intelligent Decision and Cooperative Control, Guangdong University of Technology, Guangzhou 510006, *China.*
Email: renhongru2019@gdut.edu.cn.
LI Hongyi
College of Electronic and Information Engineering and Chongqing Key Laboratory of Generic Technology and System of Service Robots, Southwest University, Chongqing 400715, *China.* Email: lihongyi2009@gmail.com.
*This work was partially supported by the National Natural Science Foundation of China under Grant Nos. 62033003, 62203119, 62373113, U23A20341, and U21A20522, and the Natural Science Foundation of Guangdong Province under Grant Nos. 2023A1515011527 and 2022A1515011506.
◇ *This paper was recommended for publication by Editor SUN Jian.*

1 Introduction

During the past years, the research on unmanned aerial vehicle (UAV) control has achieved great progress[1–4]. Due to its practical significance, uncooperative target tracking control has become a popular research topic in the field of UAV[5]. Uncooperative target maneuvers arbitrarily and cannot communicate with the tracker, i.e., the tracker cannot directly obtain target information[6]. In response, the vision-based tracking control strategy has been investigated[7]. Different from the conventional control schemes[8–10], the vision-based control method provides useful information from the target environment through the vision sensor, especially in areas where communication is poor or even not available. However, vision sensors only have access to target image information (e.g., deflection and pitch angle) but cannot directly measure relative distance. To solve this problem, some estimation methods were used to estimate the relative distance[11–13]. For ground targets[14], the relative distance was estimated from the altitude of the UAV by a coordinate system conversion. The estimation method using altitude is not available for airborne targets, while other estimation methods are required. Image feature point information is used to estimate the relative distance of the target, such as the image-based method[15] and the stereovision method[16], which require a priori information about the target. To overcome this problem, a vision-based control scheme was proposed[6], which only considers an ideal tracker. Therefore, it remains an interesting research for the UAV to track an uncooperative target when the relative distance is unknown and the priori information is lacking.

For the vision-based methods[14–16], the main attention is paid to the asymptotic stability, that is, the closed-loop system is stable as the time tends to infinity. However, for many time-sensitive applications, such as spacecraft docking and target interception, the preferred tracking accuracy needs to be achieved in finite time[17]. Sun, et al.[18] constructed a vision-based finite-time controller for UAV, where the convergence time was limited by initial values. Based on fractional plus regular state feedback, a fixed-time control approach was presented[19], which makes the settling time irrelevant to the initial value of the state. Note that fixed-time control algorithms with a state feedback component are usually difficult or even impossible to achieve stability in prescribed time. Thus, the concept of prescribed-time stability was proposed[20], which has more robust and attractive convergence performance than finite/fixed time control, i.e., the settling time can be artificially prescribed depending on the task requirements rather than determined by parameters. A prescribed finite-time control scheme was constructed with regular state feedback for specific classes of systems[21–23]. The above methods must have high energy consumption to achieve high tracking accuracy when the system has unknown disturbances and uncertainties. However, in actual tracking control, it is sufficient to achieve a prescribed range of tracking accuracy within a prescribed time. Thus, developing a practical prescribed-time control scheme for tracking system with uncertainties and unknown disturbances is of practical interest.

Due to the uncooperative feature of the target, state information can only be measured by onboard sensors, which requires that the target is always within the detectable range. Thus,

it is of great interest to determine the performance metrics (e.g., convergence rate, maximum overshoot, and stable residual set of tracking errors) in advance[24–26]. A prescribed performance control (PPC) was designed to meet the performance requirements, where the system performance could be guaranteed by the prescribed performance function[27–29]. This approach has been commonly employed in different systems due to its advantages in the transient and steady-state performances of the control system. For instance, Zhang, et al.[30] proposed a pattern-based intelligent control strategy for uncertain pure-feedback systems, where the tracking error was guaranteed in a prescribed range. However, the mentioned works require that the initial value must be predetermined within a given range, which relies on the prescribed boundary function. To remove the restriction on the initial condition, the funnel control approaches[31] and deferred PPC schemes[32] were presented, but these methods have some drawbacks. Specifically, the funnel control approach is conservative, and the deferred PPC method needs a continuous differentiable shift function. By using a time-varying scaling function, a new prescribed performance function is designed for uncertain strict-feedback nonlinear systems, which eliminates the initial condition[33]. However, in previous PPC results, the convergence time to reach the prescribed steady-state boundary could not be specified in advance. In addition, considering security and physical restrictions, constraints become one of the main problems in practical systems.

There have been many achievements in dealing with constraints[34–37]. An adaptive control scheme with the barrier Lyapunov function (BLF) was designed for nonlinear pure-feedback systems with constraints[38]. Note that if BLF is combined with the backstepping design procedure to solve the state constraint problem, the feasibility condition needs to be satisfied[39, 40]. To eliminate the demanding feasibility condition, Zhao, et al.[41] defined a nonlinear transformation function within the constrained states, and the original constrained system was converted into an equivalent unconstrained one. Following the idea proposed in [41], adaptive full-state constrained controllers were developed, such as for robust control of stochastic systems with unknown time delays[42] and nonlinear systems with unmodeled dynamics[43]. It is noticed that the above constrained researches only achieve ultimately uniform boundedness, whose settling time cannot be user-defined.

Motivated by the above discussion, this article investigates the uncooperative target tracking control problem for the UAV with unknown disturbances and performance constraint, where uncommunication and the priori information of the target are available. A vision-based adaptive prescribed-time control strategy is proposed to ensure that the UAV tracks the uncooperative target at the desired relative position within a prescribed time while satisfying all constraints during the operation. The main contributions of this article are summarized as follows: 1) Different from [8–10], the uncommunicative uncooperative target tracking problem is considered in this paper. Additionally, some difficulties associated with this problem (e.g., detectable range constraint and convergence rate requirement) are also considered, unlike existing literature[6, 18]. 2) A prescribed performance function for uncooperative target tracking is designed to guarantee tracking performance without using relative distance. In contrast to existing work on PPC[31–33], the designed prescribed performance function reaches the steady-state boundary

within a predefined time and relaxes the restrictions on the initial values. 3) An adaptive prescribed time controller is constructed for vision-based uncooperative target tracking of UAV, ensuring the practical prescribed-time stability of tracking system. Unlike the existing vision-based control schemes[18, 44–46], which only achieve finite/fixed time convergence, the setting time and tracking accuracy in this paper can be prescribed flexibly by user.

The remainder of this article is structured as follows. The problem statement and vision-based measurement are given in Section 2. The prescribed performance function is constructed in Section 3. Section 4 presents a time-varying nonlinear function that converts the constrained systems into an unconstrained nonlinear system. Then, an adaptive practical prescribed-time controller is designed to stabilize the unconstrained nonlinear system. Simulations are provided in Section 5 to validate the effectiveness of the proposed control strategy. Section 6 summarizes the conclusion of this article.

2 Problem Statement and Vision-Based Measurement

2.1 Problem Statement

This paper considers the position tracking control of UAV, where it is assumed that the attitude control of the UAV has been presented according to [15]. To better describe the relative position model, two reference frames are defined, i.e., the inertial coordinate frame $I = \{O_I, X_I, Y_I, Z_I\}$ fixed on the earth and the body-fixed reference frame $B = \{O_B, X_B, Y_B, Z_B\}$ fixed on the UAV. The rotation matrix between reference frames I and B is represented as R_B^I. The relative position model of the tracker-target is shown in Figure 1.

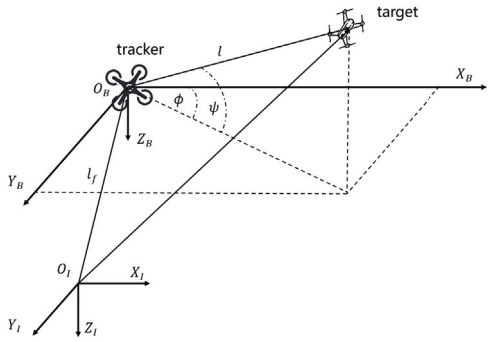

Figure 1 Relative position between target and tracker in the frame I

According to [47], we can obtain the position dynamics of the UAV as

$$\begin{aligned} \dot{l}_f &= v_f, \\ \dot{v}_f &= u_f + g\left(\overline{v}_f\right) + d, \end{aligned} \tag{1}$$

where $l_f = [l_{f,1}, l_{f,2}, l_{f,3}]^{\mathrm{T}}$ and $v_f = [v_{f,1}, v_{f,2}, v_{f,3}]^{\mathrm{T}}$ denote the position and velocity in frame I, respectively. $u_f = [u_{f,1}, u_{f,2}, u_{f,3}]^{\mathrm{T}}$ is the control input. $g\left(\overline{v}_f\right) = [g_1, g_2, g_3]^{\mathrm{T}}$ denotes the known nonlinearity function and $\overline{v}_f = \left[l_f^{\mathrm{T}}, v_f^{\mathrm{T}}\right]^{\mathrm{T}}$. $d = [d_1, d_2, d_3]^{\mathrm{T}}$ represents unknown disturbances.

The motion equation of the target is

$$\ddot{l}_t = a_t, \quad l_t(0) = l_{t0}, \quad \dot{l}_t(0) = v_{t0}, \tag{2}$$

where $l_t = [l_{t,1}, l_{t,2}, l_{t,3}]^{\mathrm{T}}$ and $a_t = [a_{t,1}, a_{t,2}, a_{t,3}]^{\mathrm{T}}$ represent the position and acceleration in frame I, respectively. l_{t0} and v_{t0} are the initial values.

In the frame I, the relative position between UAV tracker and target can be denoted as $l = l_t - l_f$, whose dynamics are given by

$$\ddot{l} = a_t - \dot{v}_f, \quad l(0) = l_0, \quad \dot{l}(0) = l_{v0}, \tag{3}$$

where l_0 and l_{v0} denote the initial values.

Assumption 2.1 (see [48]) The disturbance d_i is bounded by an unknown positive constant, that is $|d_i| < d_{i\max}$.

Assumption 2.2 (see [18]) The acceleration of target is bounded such that $|a_{t,i}| < a_{i\max}$, where $a_{i\max}$ is an unknown positive constant.

2.2 Vision-Based Measurement

Inspired by the vision-based methods of [6, 18], the UAV obtains the uncooperative target information using a vision sensor. The vision sensor is attached to the gimbal of the UAV, thus ensuring that the optical center coincides with the O_B and that the optical axis of vision sensor is parallel to the X_B. Projection model of the vision-based measurement is shown in Figure 2, where p indicates the focal length of the vision sensor.

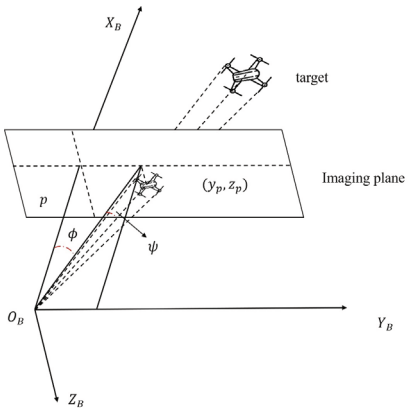

Figure 2 Vision-based measurement

Let $l_p = [p, y_p, z_p]^{\mathrm{T}}$ denote the coordinates of the target's center of gravity in the imaging plane, which is provided by the image processing algorithm associated with the vision sensor in real time. Therefore, the deflection ϕ and pitch ψ angle from the target to the tracker can be obtained as follows:

$$\tan\phi = \frac{y_p}{p}, \quad \tan\psi = \frac{z_p}{\sqrt{p^2 + y_p^2}}. \tag{4}$$

According to the principle of pinhole imaging, we can get

$$\frac{\|l_p\|}{\|l\|} = \frac{s_p}{s}, \tag{5}$$

where s_p and s are parameters associated with the size of the target in the imaging plane and in reality, respectively. $\|l_p\| = \sqrt{p^2 + y_p^2 + z_p^2}$ represents the distance between the optical center in frame B and the target's center of gravity in the imaging plane. $\|l\| = \sqrt{l_1^2 + l_2^2 + l_3^2}$ denotes the distance between the target and the tracker.

Based on (4), the relative position between UAV and target in frame B can be written as

$$l_B = \|l\| \left[C_\psi C_\phi,\ C_\psi S_\phi,\ -S_\psi\right]^{\mathrm{T}}, \tag{6}$$

where $C_* = \cos(*)$ and $S_* = \sin(*)$.

According to the rotation matrix R_B^I, the following relative position in frame I can be obtained

$$l = R_B^I l_B = \frac{s}{s_p} \|l_p\| R_B^I [C_\psi C_\phi,\ C_\psi S_\phi,\ -S_\psi]^{\mathrm{T}}. \tag{7}$$

It is noted that there is an unknown parameter s in the relative position, so we adopt the scaled relative position $r = l/s$.

$$\dot{r} = v, \quad \dot{v} = \frac{1}{s}\left(a_t - \dot{v}_f\right), \quad r\left(0\right) = r_0, \quad v\left(0\right) = v_0, \tag{8}$$

where v denotes the scaled relative velocity. $s_{\min} \leq s \leq s_{\max}$, $s_{\min}$ and $s_{\max}$ are positive parameters.

In the light of a vision sensor, the problem of an uncooperative target tracking by a UAV is reduced to the stability problem of the second-order system (8) under parameter uncertainties and unknown disturbances.

Remark 2.3 Compared with [6, 18], this paper considers a more challenging case for uncooperative target tracking control, since it involves parameter uncertainties, performance constraint, and convergence rate.

Define the scaled position error $e = r - r_d$ with $e = [e_1, e_2, e_3]^{\mathrm{T}}$ and $r_d = [r_{d,1}, r_{d,2}, r_{d,3}]^{\mathrm{T}}$. r_d represents the desired scaled relative position. $l_d = s * r_d$ is the desired relative position. Meanwhile, considering the physical constraints and Assumption 2.2, the scaled relative velocity v is required to be constrained.

The control goal of this paper is to develop a control scheme for the system (8) under the performance constraint, scaled relative velocity constraint, parameter uncertainties, and unknown disturbances, so that the UAV can follow the uncooperative target at a desired relative position within the prescribed settling time.

Then, the following lemmas are required.

Lemma 2.4 (see [49]) *Considering the system $\dot{x}(t) = f\left(x(t), t\right)$, the origin of system is practically prescribed-time stable (PPTS) if there exists a continuous-differential function*

$\Gamma(x(t),t) \geq 0$, and the following inequality is satisfied

$$\dot{\Gamma} \leq -k\Gamma - 2\frac{|\dot{\gamma}|}{\gamma}\Gamma + \frac{\rho}{\gamma} + c,$$

where $k > 0$, $0 \leq \rho < +\infty$, and $0 \leq c < +\infty$ are scalars. γ is a piecewise time-varying function, which is given by

$$\gamma = \begin{cases} \exp(o_1(T_\gamma - t)) - 1, & t \in [0, T_\gamma), \\ o_2 - o_2 \tanh(o_1(t - T_\gamma)), & t \in [T_\gamma, \infty), \end{cases} \tag{9}$$

where o_1 and o_2 are positive tunable parameters. By selecting appropriate parameters, the system trajectory will converge to the region $\Omega = \{x|\Gamma(x) \leq \rho/o_1\}$ for $t \geq T_\gamma$. For implementation, the right-hand derivative of γ at $t = T_\gamma$ is given as $\dot{\gamma}$.

Remark 2.5 As shown in (9), the parameters T_γ, o_1, and o_2 are used to describe the control performance. The parameter T_γ presents the convergence time, which is not related to initial values or design parameters. The user can define the convergence time and convergence region according to the practical tasks. Furthermore, it can be seen that the convergence region Ω of the system is related to o_1, i.e., the larger o_1 the smaller the convergence region. However, an excessively large o_1 will result in an excessive control signal, so that a trade-off needs to be made between system performance and physically achievable ranges. According to [49], the parameters are set as $o_1 \in (0.5, 1)$ and $o_2 = 1$, which guarantees the continuity of the $\dot{\gamma}$.

Lemma 2.6 (see [33]) *For any positive constants h, b and scalar x, the following function*

$$H(x) = \frac{\sqrt{b}x}{\sqrt{h^2 - x^2}}$$

is increasing strictly monotonically in the interval $(-h, h)$.

Lemma 2.7 (see [45]) *Considering $x \in R$, for any $\delta > 0$, the following inequality hold*

$$0 \leq |x| < \delta + \frac{x^2}{\sqrt{x^2 + \delta^2}}.$$

3 Prescribed Performance Constraint

The transient and steady-state characterizations are essential performance indicators of the control system. In order to predefine certain behaviors of the scaled position error e, we further restrict e to evolve within a specified range.

To reach the desired steady-state performance within a prescribed time, the following time-varying constraining function is developed

$$\mu_{1,i}(t) = \begin{cases} (\mu_{0,i} - \mu_{\infty,i}) \exp\left(\dfrac{-t}{T_\mu - t}\right) + \mu_{\infty,i}, & t \in [0, T_\mu), \\ \mu_{\infty,i}, & t \in [T_\mu, \infty), \end{cases} \tag{10}$$

where $i = 1, 2, 3$ and $\mu_{0,i} > \mu_{\infty,i} > 0$. Define $\mu_0 = [\mu_{0,1}, \mu_{0,2}, \mu_{0,3}]^{\mathrm{T}}$, $\mu_\infty = [\mu_{\infty,1}, \mu_{\infty,2}, \mu_{\infty,3}]^{\mathrm{T}}$ and $\mu_1 = [\mu_{1,1}, \mu_{1,2}, \mu_{1,3}]^{\mathrm{T}}$. Note that $\mu_{1,i}(t)$ is monotonically decreasing and $\mu_{1,i}(0) = \mu_{0,i}$. $T_\mu \in (0, \infty)$ is a prescribed settling time, that is, $\lim_{t\to T_\mu} \mu_{1,i}(t) = \mu_{\infty,i}$.

Upon utilizing (10), the prescribed performance function is as follows:

$$H(\mu_{1,i}) = \frac{\sqrt{b_i}\mu_{1,i}}{\sqrt{\mu_{0,i}^2 - \mu_{1,i}^2}}, \tag{11}$$

where $b_i = \mu_{0,i}^2 - \mu_{\infty,i}^2$. Then one has $H(\mu_{0,i}) = \infty$ and $\lim_{t\to T_\mu} H(\mu_{1,i}) = \mu_{\infty,i}$.

The prescribed performance constraint on the scaled distance error e_i is as follows

$$-H(\mu_{1,i}) < e_i < H(\mu_{1,i}), \tag{12}$$

with

$$\begin{cases} -\infty < e_i < \infty, & t = 0, \\ -\dfrac{\sqrt{b_i}\mu_{1,i}}{\sqrt{\mu_{0,i}^2 - \mu_{1,i}^2}} < e_i < \dfrac{\sqrt{b_i}\mu_{1,i}}{\sqrt{\mu_{0,i}^2 - \mu_{1,i}^2}}, & t \in (0, T_\mu), \\ -\mu_{\infty,i} < e_i < \mu_{\infty,i}, & t \in [T_\mu, \infty). \end{cases} \tag{13}$$

Remark 3.1 In [24], the traditional prescribed performance function is selected as $h_i(t) = (h_{0,i} - h_{\infty,i})\exp(-\imath t) + h_{\infty,i}$, which only ensures that the tracking error enters into the predetermined region $(-h_{\infty,i}, h_{\infty,i})$ as the time t tends to infinity. Besides, this method requires the initial value of tracking error to meet the condition $-h_i(0) < e_i(0) < h_i(0)$. Thus, an improved prescribed performance function (11) is proposed in this paper. If (12) holds, the scaled distance error e_i will converge to a prescribed region $(-\mu_{\infty,i}, \mu_{\infty,i})$ within a prescribed time T_μ and removes the restriction on $e_i(0)$.

As shown in (12), the restriction on the initial value is eliminated. To ensure the prescribed performance, the following nonlinear shifting function is adopted

$$G(e_i) = \frac{\mu_{0,i} e_i}{\sqrt{e_i^2 + b_i}}, \tag{14}$$

where $G(e_i) \in (-\mu_{0,i}, \mu_{0,i})$. The derivative of $G(e_i)$ is $\dot{G}(e_i) = \mu_{0,i} b_i \dot{e}_i / \left(e_i^2 + b_i\right)^{3/2}$. Note that the monotonicity of $G(e_i)$ is related to e_i. When $G(e_i) \to \pm\mu_{0,i}$, we can obtain $e_i \to \pm\infty$. The initial value $e_i(0)$ can be arbitrarily chosen.

With the help of (10) and (14), we define a transformation function as

$$\xi_{1,i} = \frac{G(e_i)}{\mu_{1,i}}, \tag{15}$$

where $\xi_{1,i}(0) = G(e_i(0))/\mu_{0,i} \in (-1, 1)$, indicating that the initial value $\xi_{1,i}(0)$ is explicit. In addition, $\dot{\xi}_{1,i} = \dot{G}(e_i)/\mu_{1,i} - G(e_i)\dot{\mu}_{1,i}/\mu_{1,i}^2$.

Lemma 3.2 *If there exists a constant* $0 < \overline{\xi}_{1,i} < 1$ *with* $|\xi_{1,i}| < \overline{\xi}_{1,i}$, *the prescribed performance* (12) *is satisfied.*

Proof Suppose that $|\xi_{1,i}| < \overline{\xi}_{1,i}$, such that

$$-\mu_{1,i} < -\overline{\xi}_{1,i}\mu_{1,i} < G(e_i) < \overline{\xi}_{1,i}\mu_{1,i} < \mu_{1,i}.$$

From the definition of $H(x)$, one obtains

$$-H(\mu_{1,i}) < H(G(e_i)) < H(\mu_{1,i}).$$

Based on (14), the scaled distance error can be written as

$$e_i = \frac{\sqrt{b_i}G(e_i)}{\sqrt{\mu_{0,i}^2 - G^2(e_i)}} = H(G(e_i)).$$

Hence, (12) holds. The proof is completed. ∎

Then, the tracking control problem with prescribed performance can be achieved simultaneously as long as $|\xi_{1,i}| < \overline{\xi}_{1,i} < 1$ is satisfied. In addition, the scaled relative velocity is constrained by the time-varying positive functions $\overline{\mu}_{2,i}$ and $\underline{\mu}_{2,i}$, that is, $-\underline{\mu}_{2,i} < v_i < \overline{\mu}_{2,i}$.

4 Controller Design

4.1 System Transformation

The problem of constraints is far from trivial, especially when the boundaries of the constraints are asymmetrical and time-varying. A time-varying nonlinear function is introduced to tackle the issue of state constraints. By means of this transformation function, the constrained system (8) is reformulated as an unconstrained system whose stability ensures the constraints of the $\xi_{1,i}$ and v_i.

Consider the following time-varying nonlinear transformed function

$$\chi_{1,i} = \frac{\xi_{1,i}}{1 - \xi_{1,i}^2}, \tag{16}$$

$$\chi_{2,i} = \frac{v_i\overline{\mu}_{2,i}\underline{\mu}_{2,i}}{\left(\underline{\mu}_{2,i} + v_i\right)\left(\overline{\mu}_{2,i} - v_i\right)}. \tag{17}$$

Thus, the problem of constraints is transformed into ensuring the boundedness of $\chi_{j,i}$, $j = 1, 2$.

Remark 4.1 It is worth noticing that the time-varying nonlinear transformed function in $\chi_{2,i}$ is characterized by a finite escape as the v_i approaches the defined error bounds $-\underline{\mu}_{2,i}$ or $\overline{\mu}_{2,i}$, that is, $\lim_{v_i \to \overline{\mu}_{2,i}} \chi_{2,i} = \infty$ and $\lim_{v_i \to -\underline{\mu}_{2,i}} \chi_{2,i} = -\infty$. Furthermore, if the transformed errors are unconstrained, one can obtain $\lim_{\overline{\mu}_{2,i} = \underline{\mu}_{2,i} \to \infty} \chi_{2,i} = v_i$. As a result, it is concluded that the proposed time-varying nonlinear transformed function can cope with symmetric or asymmetric constraints, and it can be used for systems without constraint requirements.

From (17), one obtains $v_i = \eta_{2,i}\chi_{2,i}$ with $\eta_{2,i} = (\underline{\mu}_{2,i} + v_i)(\overline{\mu}_{2,i} - v_i)/(\underline{\mu}_{2,i}\overline{\mu}_{2,i})$ being a positive function. There exists a positive constant $\overline{\eta}_{2,i}$ such that $0 < \eta_{2,i} < \overline{\eta}_{2,i} < \infty$.

Based on (16) and (17), the time derivatives of $\chi_{1,i}$ and $\chi_{2,i}$ are given by

$$\dot{\chi}_{1,i} = \chi_{11,i}\dot{e}_i + \chi_{12,i}, \quad \dot{\chi}_{2,i} = \chi_{21,i}\dot{v}_i + \chi_{22,i}, \tag{18}$$

with

$$\begin{aligned}
\chi_{11,i} &= \frac{\left(1+\xi_{1,i}^2\right) G_{1,i}}{\left(1-\xi_{1,i}^2\right)\mu_{1,i}},\\
\chi_{12,i} &= -\frac{\left(1+\xi_{1,i}^2\right)\dot{\mu}_{1,i}\xi_{1,i}}{\left(1-\xi_{1,i}^2\right)\mu_{1,i}},\\
\chi_{21,i} &= \frac{\underline{\mu}_{2,i}\overline{\mu}_{2,i}\left(\underline{\mu}_{2,i}\overline{\mu}_{2,i}+v_i^2\right)}{\left(\underline{\mu}_{2,i}+v_i\right)^2\left(\overline{\mu}_{2,i}-v_i\right)^2},\\
\chi_{22,i} &= \frac{v_i^2\left(\dot{\underline{\mu}}_{2,i}\overline{\mu}_{2,i}^2-\underline{\mu}_{2,i}^2\dot{\overline{\mu}}_{2,i}\right)-v_i^3\left(\dot{\underline{\mu}}_{2,i}\overline{\mu}_{2,i}+\underline{\mu}_{2,i}\dot{\overline{\mu}}_{2,i}\right)}{\left(\underline{\mu}_{2,i}+v_i\right)^2\left(\overline{\mu}_{2,i}-v_i\right)^2},
\end{aligned}$$

where $G_{1,i} = \mu_{0,i}b_i/\left(e_i^2+b_i\right)^{3/2}$, $\underline{\mu}_{2,i} > 0$ and $\overline{\mu}_{2,i} > 0$. Then, we have $\chi_{11,i} > 0$ and $\chi_{21,i} > 0$.

Substituting (8) into (18), the newly transformed system can be presented as

$$\begin{aligned}
\dot{\chi}_{1,i} &= \chi_{11,i}\eta_{2,i}\chi_{2,i} + \chi_{12,i},\\
\dot{\chi}_{2,i} &= \frac{\chi_{21,i}}{s}\left(a_{t,i} - u_{f,i} - g_i - d_i\right) + \chi_{22,i}.
\end{aligned} \tag{19}$$

Therefore, the prescribed performance constraint problem for e_i and the constraint problem for v_i are transformed into the problem of making the states $\chi_{1,i}$ and $\chi_{2,i}$ bounded. Then, the goal of this paper is to stabilize the transformed system (19) by the design of the controller $u_{f,i}$.

4.2 Controller Design

An adaptive prescribed-time controller is developed for the transformed system (19) with unknown disturbances and parameter uncertainties within the backstepping framework.

According to (19), the coordinate transformations are constructed as

$$\begin{aligned}
z_{1,i} &= \chi_{1,i},\\
z_{1,i} &= \chi_{2,i} - \omega_{1f,i},
\end{aligned} \tag{20}$$

with $\omega_{1f,i}$ being the output of first-order filter, which is given as follows:

$$\omega_{s,i}\dot{\omega}_{1f,i} + \omega_{1f,i} = \eta_{2,i}^{-1}\omega_{1,i}, \tag{21}$$

where $\omega_{s,i}$ is a positive constant. Define the boundary layer error $e_{\omega,i} = \omega_{1f,i} - \eta_{2,i}^{-1}\omega_{1,i}$. The intermediate control function $\omega_{1,i}$ is designed as

$$\begin{aligned}
\omega_{1,i} &= -\frac{z_{1,i}\overline{\omega}_{1,i}^2}{\chi_{11,i}\sqrt{z_{1,i}^2\overline{\omega}_{1,i}^2+\tau_{1,i}^2}},\\
\overline{\omega}_{1,i} &= z_{1,i}\chi_{11,i}^2 + \chi_{12,i} + \frac{1}{2}\alpha_{1,i}z_{1,i} - h\left(z_{1,i}\right)\frac{\rho_i}{\gamma},
\end{aligned} \tag{22}$$

where $\alpha_{1,i} = k_{1,i} + \frac{2|\dot{\gamma}|}{\gamma}$. $k_{1,i}$, $\tau_{1,i}$, and ρ_i are positive design parameters. γ is designed from Lemma 2.4. For arbitrary small $\delta_1 > 0$, we have $h(z_{1,i}) = \xi(z_{1,i})/z_{1,i}$ with

$$\xi(z_{1,i}) = \begin{cases} \sin\left(\dfrac{\pi |z_{1,i}|}{2\delta}\right), & |z_{1,i}| \le \delta_1, \\ 1, & \text{else.} \end{cases}$$

Remark 4.2 According to L'Hopital rule, the switching property of $\xi(z_i)$ ensures the smoothness characteristic of $h(z_i)$, that is, $\lim_{z_i \to 0^+} h(z_i) = \pi/2\delta_1$ and $\lim_{z_i \to 0^-} h(z_i) = -\pi/2\delta_1$.

The actual controller is constructed as

$$\begin{aligned} u_{f,i} =& \frac{s_{\max} z_{2,i} \overline{\omega}_{2,i}^2}{\chi_{21,i} \sqrt{z_{2,i}^2 \overline{\omega}_{2,i}^2 + \tau_{2,i}^2}}, \\ \overline{\omega}_{2,i} =& \frac{\widehat{\theta}_{1,i} z_{2,i} \chi_{21,i}^2}{2 q_{1,i}^2 s_{\min}^2} + \frac{z_{2,i} \chi_{21,i}^2 g_i^2}{s_{\max} \sqrt{z_{2,i}^2 \chi_{21,i}^2 g_i^2 + \sigma_i^2}} + \chi_{22,i} - \dot{\omega}_{1f,i} + \frac{\eta_{2,i}^2 z_{2,i}}{2} + \frac{1}{2} \alpha_{2,i} z_{2,i}, \end{aligned} \tag{23}$$

where $\alpha_{2,i} = k_{2,i} + \frac{2|\dot{\gamma}|}{\gamma}$. $k_{2,i}$, $\tau_{2,i}$, $q_{1,i}$, and σ_i are positive parameters. $\widehat{\theta}_{1,i}$ denotes the estimation of $\theta_{1,i}$, which is updated by

$$\dot{\widehat{\theta}}_{1,i} = \frac{r_{1,i} z_{2,i}^2 \chi_{21,i}^2}{2 q_{1,i}^2 s_{\min}^2} - \alpha_{3,i} \widehat{\theta}_{1,i}, \tag{24}$$

with $\alpha_{3,i} = k_{3,i} + \frac{2|\dot{\gamma}|}{\gamma}$. $r_{1,i}$ and $k_{3,i}$ being positive parameters.

Remark 4.3 The PPTS is achieved by employing a control gain that will reach ∞ as $t \to T_\gamma$, while ensuring that the states of system are bounded. Exploiting unbounded control gain can be traced to early research in terminal sliding mode methods, optimal control and time-based generators[21–23]. For implementation purposes, several solutions can be used, such as adding a small constant γ_l^2 to the denominator of $1/\gamma$ to avoid the singularity when $t \to T_\gamma$ or using the dynamic damping reciprocal (DDR) method[50].

Then, the main results are recapitulated in Theorem 4.4.

Theorem 4.4 *Consider the tracker-target system* (8) *under prescribed performance constraint* (12)*, scaled relative velocity constraints, parameter uncertainties, and unknown disturbances. The proposed control strategies* (22)–(24) *can guarantee that* 1) *all signals of the closed-loop system are bounded;* 2) *the constraints of* $\xi_{1,i}$ *and* v_i *are not violated all the time;* 3) *the scaled distance error* e_i *evolves strictly within the prescribed performance range given by* (12) *and converges to prescribed region within the prescribed time;* 4) *the tracker UAV tracks the uncooperative target with a desired position.*

Proof **Step 1** Define the Lyapunov function candidate as $\Gamma_{1,i} = 0.5 z_{1,i}^2$, and its derivative with respect to time is

$$\dot{\Gamma}_{1,i} = z_{1,i} (\chi_{11,i} \eta_{2,i} \chi_{2,i} + \chi_{12,i}). \tag{25}$$

Based on (20) and $e_{\omega,i}$, (25) can be written as

$$\dot{\Gamma}_{1,i} = z_{1,i}\left(\chi_{11,i}\eta_{2,i}\left(z_{2,i} + e_{\omega,i} + \eta_{2,i}^{-1}\omega_{1,i}\right) + \chi_{12,i}\right). \tag{26}$$

According to Young's inequality, one obtains

$$\begin{aligned} z_{1,i}\chi_{11,i}\eta_{2,i}z_{2,i} &\leq \frac{z_{1,i}^2\chi_{11,i}^2}{2} + \frac{\eta_{2,i}^2 z_{2,i}^2}{2}, \\ z_{1,i}\chi_{11,i}\eta_{2,i}e_{\omega,i} &\leq \frac{z_{1,i}^2\chi_{11,i}^2}{2} + \frac{\eta_{2,i}^2 e_{\omega,i}^2}{2}. \end{aligned} \tag{27}$$

Then, we have

$$\dot{\Gamma}_{1,i} \leq z_{1,i}\left(\chi_{11,i}^2 z_{1,i} + \chi_{11,i}\omega_{1,i} + \chi_{12,i}\right) + \frac{\eta_{2,i}^2 z_{2,i}^2}{2} + \frac{\eta_{2,i}^2 e_{\omega,i}^2}{2}. \tag{28}$$

From Lemma 2.7 and (22), one has

$$z_{1,i}\chi_{11,i}\omega_{1,i} \leq \tau_{1,i} - z_{1,i}^2\chi_{11,i}^2 - z_{1,i}\chi_{12,i} - \frac{1}{2}\alpha_{1,i}z_{1,i}^2 + \frac{\rho_i}{\gamma}. \tag{29}$$

Substituting (29) into (28) yields

$$\dot{\Gamma}_{1,i} \leq -\frac{1}{2}\alpha_{1,i}z_{1,i}^2 + \frac{\rho_i}{\gamma} + \tau_{1,i} + \frac{\eta_{2,i}^2 z_{2,i}^2}{2} + \frac{\eta_{2,i}^2 e_{\omega,i}^2}{2}. \tag{30}$$

Then, from (30) and Lemma 2.4, it can be seen that the PPTS property of $z_{1,i}$ can be ensured if $z_{2,i}$ and $e_{\omega,i}$ are stabilized.

Step 2 Construct the following Lyapunov function

$$\Gamma_{2,i} = \Gamma_{1,i} + \frac{1}{2}z_{2,i}^2 + \frac{1}{2r_{1,i}}\widetilde{\theta}_{1,i}^2 + \frac{1}{2}e_{\omega,i}^2, \tag{31}$$

where $\widetilde{\theta}_{1,i} = \theta_{1,i} - \widehat{\theta}_{1,i}$ is estimation error. Based on (20), $\dot{\Gamma}_{2,i}$ can be calculated as

$$\dot{\Gamma}_{2,i} = \dot{\Gamma}_{1,i} + z_{2,i}\left(\dot{\chi}_{2,i} - \dot{\omega}_{1f,i}\right) - \frac{\widetilde{\theta}_{1,i}\dot{\widehat{\theta}}_{1,i}}{r_{1,i}} + e_{\omega,i}\dot{e}_{\omega,i}. \tag{32}$$

According to (19) and (20), it follows from (32) that

$$\begin{aligned} \dot{\Gamma}_{2,i} =& \dot{\Gamma}_{1,i} + z_{2,i}\left(\chi_{21,i}\dot{v}_i + \chi_{22,i} - \dot{\omega}_{1f,i} + \frac{\eta_{2,i}^2 z_{2,i}}{2}\right) - \frac{1}{r_{1,i}}\widetilde{\theta}_{1,i}\dot{\widehat{\theta}}_{1,i} - \frac{\eta_{2,i}^2 z_{2,i}^2}{2} + e_{\omega,i}\dot{e}_{\omega,i} \\ =& \dot{\Gamma}_{1,i} - \frac{\eta_{2,i}^2 z_{2,i}^2}{2} + z_{2,i}\left(\frac{\chi_{21,i}\left(a_{t,i} - d_i\right)}{s} - \frac{\chi_{21,i}u_{f,i}}{s} - \frac{\chi_{21,i}g_i}{s} - \dot{\omega}_{1f,i} + \chi_{22,i} + \frac{\eta_{2,i}^2 z_{2,i}}{2}\right) \\ & - \frac{1}{r_{1,i}}\widetilde{\theta}_{1,i}\dot{\widehat{\theta}}_{1,i} + e_{\omega,i}\dot{e}_{\omega,i}. \end{aligned} \tag{33}$$

Based on (21) and the definition of $e_{\omega,i}$, one obtains $\dot{e}_{\omega,i} = -\omega_{s,i}^{-1}e_{\omega,i} + \varsigma_i$, $\varsigma_i = \eta_{2,i}^{-2}\omega_{1,i}\dot{\eta}_{2,i} - \eta_{2,i}^{-1}\dot{\omega}_{1,i}$ and $\dot{\omega}_{1,i} = \left(\chi_{11,i}\eta_{2,i}\chi_{2,i} + \chi_{12,i}\right)\partial\omega_{1,i}/\partial\chi_{1,i} + \dot{\xi}_{1,i}\partial\omega_{1,i}/\partial\xi_{1,i} + \dot{\mu}_{1,i}\partial\omega_{1,i}/\partial\mu_{1,i} + \dot{e}_i\partial\omega_{1,i}/\partial e_i$. Then, we have

$$e_{\omega,i}\dot{e}_{\omega,i} \leq \left(\frac{1}{4} - \frac{1}{\omega_{s,i}}\right)e_{\omega,i}^2 + \varsigma_i^2. \tag{34}$$

With the help of Assumptions 2.1 and 2.2, and Young's inequality, we have

$$\frac{z_{2,i}\chi_{21,i}a_i}{s} \le \frac{z_{2,i}^2\chi_{21,i}^2a_i^2}{2q_{1,i}^2s^2} + \frac{q_{1,i}^2}{2} \le \frac{z_{2,i}^2\chi_{21,i}^2a_{i\max}^2}{2q_{1,i}^2s_{\min}^2} + \frac{q_{1,i}^2}{2},$$

$$\frac{-z_{2,i}\chi_{21,i}d_i}{s} \le \frac{z_{2,i}^2\chi_{21,i}^2d_i^2}{2q_{1,i}^2s^2} + \frac{q_{1,i}^2}{2} \le \frac{z_{2,i}^2\chi_{21,i}^2d_{i\max}^2}{2q_{1,i}^2s_{\min}^2} + \frac{q_{1,i}^2}{2}. \tag{35}$$

Applying Lemma 2.7, one can obtain

$$-\frac{z_{2,i}\chi_{21,i}g_i}{s} \le \frac{z_{2,i}^2\chi_{21,i}^2g_i^2}{s_{\max}\sqrt{z_{2,i}^2\chi_{21,i}^2g_i^2+\sigma_i^2}} + \frac{\sigma_i}{s_{\max}}. \tag{36}$$

Substituting (34) and (36) into (33) yields

$$\begin{aligned}\dot{\Gamma}_{2,i} \le& \dot{\Gamma}_{1,i} + z_{2,i}\left(\frac{z_{2,i}\chi_{21,i}^2\left(a_{i\max}^2+d_{i\max}^2\right)}{2q_{1,i}^2s_{\min}^2} + \frac{z_{2,i}\chi_{21,i}^2g_i^2}{s_{\max}\sqrt{z_{2,i}^2\chi_{21,i}^2g_i^2+\sigma_i^2}} - \frac{\chi_{21,i}u_{f,i}}{s} + \chi_{22,i}\right.\\ &\left.-\dot{\omega}_{1f,i} + \frac{\eta_{2,i}^2z_{2,i}}{2}\right) + \left(\frac{1}{4} - \frac{1}{\omega_{s,i}} + \frac{\eta_{2,i}^2}{2}\right)e_{\omega,i}^2 - \frac{1}{r_{1,i}}\widetilde{\theta}_{1,i}\dot{\widehat{\theta}}_{1,i} - \frac{\eta_{2,i}^2z_{2,i}^2}{2} - \frac{\eta_{2,i}^2e_{\omega,i}^2}{2} + \frac{\sigma_i}{s_{\max}}\\ &+\varsigma_i^2 + q_{1,i}^2.\end{aligned} \tag{37}$$

Define $\theta_{1,i} = a_{i\max}^2 + d_{i\max}^2$ and $c_{1,i} = q_{1,i}^2 + \sigma_i/s_{\max} + \varsigma_i^2$. In addition, $\frac{1}{\omega_{s,i}} \ge \frac{1}{4} + \frac{\eta_{2,i}^2}{2} + \frac{1}{2}\alpha_{4,i}$ with $\alpha_{4,i} = k_{4,i} + \frac{2|\dot{\gamma}|}{\gamma}$. Then (37) can be written as

$$\begin{aligned}\dot{\Gamma}_{2,i} \le& \dot{\Gamma}_{1,i} + z_{2,i}\left(\frac{\widehat{\theta}_{1,i}z_{2,i}\chi_{21,i}^2}{2q_{1,i}^2s_{\min}^2} - \dot{\omega}_{1f,i} + \frac{\eta_{2,i}^2z_{2,i}}{2} + \frac{z_{2,i}\chi_{21,i}^2g_i^2}{s_{\max}\sqrt{z_{2,i}^2\chi_{21,i}^2g_i^2+\sigma_i^2}} - \frac{\chi_{21,i}u_{f,i}}{s} + \chi_{22,i}\right)\\ &- \frac{\widetilde{\theta}_{1,i}}{r_{1,i}}\left(\frac{r_{1,i}z_{2,i}^2\chi_{21,i}^2}{2q_{1,i}^2s_{\min}^2} - \dot{\widehat{\theta}}_{1,i}\right) - \frac{1}{2}\alpha_{4,i}e_{\omega,i}^2 - \frac{\eta_{2,i}^2z_{2,i}^2}{2} - \frac{\eta_{2,i}^2e_{\omega,i}^2}{2} + c_{1,i}.\end{aligned} \tag{38}$$

From (23), one obtains

$$\begin{aligned}&-\frac{\chi_{21,i}u_{f,i}}{s}\\ \le& -\frac{z_{2,i}^2\overline{\omega}_{2,i}^2}{\sqrt{z_{2,i}^2\overline{\omega}_{2,i}^2+\tau_{2,i}^2}}\\ \le& \tau_{2,i} - \frac{\widehat{\theta}_{1,i}z_{2,i}^2\chi_{21,i}^2}{2q_{1,i}^2s_{\min}^2} - \frac{z_{2,i}^2\chi_{21,i}^2g_i^2}{s_{\max}\sqrt{z_{2,i}^2\chi_{21,i}^2g_i^2+\sigma_i^2}} - \frac{1}{2}\alpha_{2,i}z_{2,i}^2 - z_{2,i}\chi_{22,i} + z_{2,i}\dot{\omega}_{1f,i} - \frac{\eta_{2,i}^2z_{2,i}^2}{2}.\end{aligned} \tag{39}$$

Based on (24), (30), and (39), we get from (38) that

$$\dot{\Gamma}_{2,i} \le -\frac{1}{2}\alpha_{1,i}z_{1,i}^2 - \frac{1}{2}\alpha_{2,i}z_{2,i}^2 + \frac{1}{r_{1,i}}\alpha_{3,i}\widetilde{\theta}_{1,i}\widehat{\theta}_{1,i} - \frac{1}{2}\alpha_{4,i}e_{\omega,i}^2 + \frac{\rho_i}{\gamma} + c_{1,i} + \tau_{1,i} + \tau_{2,i}. \tag{40}$$

Using Young's inequality, one has

$$\widetilde{\theta}_{1,i}\widehat{\theta}_{1,i} \leq \frac{1}{2}\theta_{1,i}^2 - \frac{1}{2}\widetilde{\theta}_{1,i}^2. \tag{41}$$

Substituting (41) into (40) yields

$$\dot{\Gamma}_{2,i} \leq -\alpha_{1,i}\frac{1}{2}z_{1,i}^2 + \frac{\rho_i}{\gamma} - \alpha_{2,i}\frac{1}{2}z_{2,i}^2 - \alpha_{3,i}\frac{1}{2r_{1,i}}\widetilde{\theta}_{1,i}^2 - \alpha_{4,i}\frac{1}{2}e_{\omega,i}^2 + c_{2,i}, \tag{42}$$

with

$$c_{2,i} = \frac{1}{2r_{1,i}}\alpha_{3,i}\theta_{1,i}^2 + c_{1,i} + \tau_{1,i} + \tau_{2,i}.$$

Note that the overall Lyapunov function is $\Gamma_2 = \sum_i^3 \Gamma_{2,i}$ and its derivative is as

$$\dot{\Gamma}_2 \leq -\left(k + \frac{2\,|\dot{\gamma}|}{\gamma}\right)\Gamma_2 + \frac{\rho}{\gamma} + c, \tag{43}$$

where $c = \sum_{i=1}^3 c_{2,i}$, $i = 1, 2, 3$, $\rho = \max\{\rho_i\}$, and $k = \min\{k_{1,i}, k_{2,i}, k_{3,i}\}$.

Theorem 4.4 can be obtained and verified as follows:

1) In the view of Lemma 2.4, the PPTS characteristic of the closed-loop system is expressed, which means the boundedness of $z_{1,i} = \chi_{1,i}$, $z_{2,i}$, $e_{\omega,i}$, and $\widetilde{\theta}_{1,i}$ can be guaranteed over the interval $t \in [0, T_\gamma)$. When $t \geq T_\gamma$, the trajectory of the system converges to a prescribed region such that $\Gamma_1 < \Gamma_2 \leq \rho/o_1 = \overline{\Gamma}_2$. From (16), the boundary of $\xi_{1,i}$ can be further reduced as $|\xi_{1,i}| < \overline{\xi}_{1,i}$ with $\overline{\xi}_{1,i} \leq \sqrt{\frac{2\overline{\Gamma}_2}{1+2\overline{\Gamma}_2}}$. Since $z_{1,i}$, $e_{\omega,i}$, $\xi_{1,i}$, $\mu_{1,i}$, and $\eta_{2,i}^{-1}$ are bounded, it is not difficult to get that $\omega_{1,i}$ and $\omega_{1f,i}$ are bounded.

2) According to the definition of $\xi_{1,i}$ in (10), it can be concluded that e_i will strictly evolve within the prescribed performance range given by (12). Then, it can be concluded that the scaled distance errors reach the steady-state boundary $\Omega_1 = \{-\mu_{\infty,i} < e_i < \mu_{\infty,i}, i = 1, 2, 3\}$ within a prescribed time T_μ satisfied $T_\mu < T_\gamma$. Since $z_{2,i}$, $\overline{\mu}_{2,i}$, $\underline{\mu}_{2,i}$, $\omega_{1f,i}$, $\eta_{2,i}$ are bounded, $\chi_{2,i}$ and $u_{f,i}$ are bounded and v_i is no violating state constraint $-\underline{\mu}_{2,i} < v_i < \overline{\mu}_{2,i}$.

3) Under the proposed control scheme, the tracker UAV tracks the uncooperative target within prescribed performance while maintaining the desired relative position.

For readability purposes, the proposed vision-based adaptive prescribed-time control block diagram is depicted in Figure 3. Defined $\xi_1 = [\xi_{1,1}, \xi_{1,2}, \xi_{1,3}]^{\mathrm{T}}$, $\chi_1 = [\chi_{1,1}, \chi_{1,2}, \chi_{1,3}]^{\mathrm{T}}$, $\chi_2 = [\chi_{2,1}, \chi_{2,2}, \chi_{2,3}]^{\mathrm{T}}$, $\theta_1 = [\theta_{1,1}, \theta_{1,2}, \theta_{1,3}]^{\mathrm{T}}$, $\omega_{1f} = [\omega_{1f,1}, \omega_{1f,2}, \omega_{1f,3}]^{\mathrm{T}}$, and $\omega_1 = [\omega_{1,1}, \omega_{1,2}, \omega_{1,3}]^{\mathrm{T}}$.

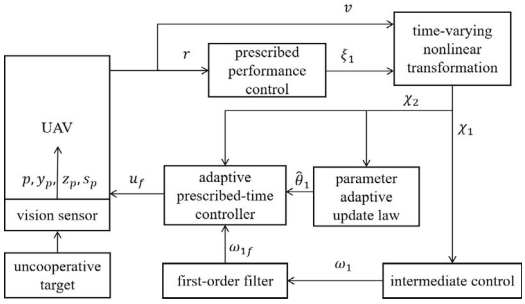

Figure 3 Block diagram of the proposed vision-based adaptive prescribed-time control scheme

5 Simulation

To demonstrate the effectiveness of the vision-based adaptive prescribed-time control scheme with prescribed performance, the simulation examples are carried out. Some parameters of UAV and target are listed in Table 1.

Table 1 Parameter setting

Parameter	Value
Initial values of target	$l_t(0) = [50, 30, 4]^{\mathrm{T}}$ m, $v_t(0) = [4, 2, 1]^{\mathrm{T}}$ m/s
Initial values of tracker	$l_f(0) = [0, 0, 0]^{\mathrm{T}}$ m, $v_f(0) = [0, 0, 0]^{\mathrm{T}}$ m/s
Focal length of the camera	$p = 12$ mm
Size of the target	$s = 0.7$ m
Desired scaled relative position	$r_d = [2.1, 0, 0]^{\mathrm{T}}$ m
Model nonlinearity	$g_i = v_{f,i} \sin(l_{f,i})$
Disturbances	$d_i = 2\sin(t)$
Parameters of PPTS	$o_1 = 0.6,\ o_2 = 1,\ \rho = 0.001,\ T_\gamma = 15$ s
Parameters of controller	$k_1 = [2, 8, 0.1, 5]^{\mathrm{T}}$ $k_2 = [1, 8, 0.1, 5]^{\mathrm{T}}$ $k_3 = [1.2, 8, 0.1, 5]^{\mathrm{T}}$ $r_{1,i} = 0.1,\ \tau_{1,i} = \tau_{2,i} = 0.001$ $q_1 = [10, 10, 10]^{\mathrm{T}},\ \delta_1 = 0.01$

By taking into account the arbitrary maneuvering of the uncooperative target, the acceleration of the target is set as a segmentation function $a_t = a_0 + \Delta$, where

$$a_0 = \begin{cases} [1, -0.2, 0.2]^{\mathrm{T}}\ \mathrm{m/s^2}, & 0\ \mathrm{s} \le t < 5\ \mathrm{s}, \\ [-0.2, 1.4, -0.5]^{\mathrm{T}}\ \mathrm{m/s^2}, & 18\ \mathrm{s} \le t < 20\ \mathrm{s}, \\ [0, -1.4, 0]^{\mathrm{T}}\ \mathrm{m/s^2}, & 28\ \mathrm{s} \le t < 30\ \mathrm{s}, \\ [0, 0, 0]^{\mathrm{T}}\ \mathrm{m/s^2}, & \mathrm{else}, \end{cases}$$

$$\Delta = 0.05\left[\sin\left(\frac{\pi t}{30}\right), \sin\left(\frac{\pi t}{30}\right), \sin\left(\frac{\pi t}{30}\right)\right]^{\mathrm{T}}\ \mathrm{m/s^2}.$$

Set the parameters of the prescribed performance as $\mu_0 = [47, 30, 13]^{\mathrm{T}}$ m, $T_\mu = 5$ s and $\mu_\infty = [0.5, 0.5, 0.5]^{\mathrm{T}}$ m. The constraints on the scaled relative velocities are defined as $\underline{\mu}_{2,i} = 50 - 20\ \sin(t)$ and $\overline{\mu}_{2,i} = 140 - 56\ \sin(t)$. A pinhole camera is used to provide target information through the associated image processing algorithm. The visual processing and tracking algorithm are set at rates of 30 Hz and 100 Hz, respectively. Note that the vision processing detection and tracking algorithms have different frame rates in practice, which can be handled by linear interpolation.

The results of the simulation are presented in Figures 4–9. Figure 4 and Figure 5 represent the tracker-target trajectories in the two-dimensional plane and three-dimensional plane,

respectively. The curves of relative distance and relative velocity are plotted in Figure 6 and Figure 7, respectively. As shown in Figures 4–7, it can be concluded that the relative position l and the relative velocity l_v arrive within a very small region of the desired value in time T_γ. The scaled distance errors e_i under the proposed controller are shown in Figure 8 with the prescribed performance function $\mu_{1,i}$, where e_i evolves within the prescribed performance range and converges to $\Omega_1 = \{-0.5 < e_i < 0.5, i = 1, 2, 3\}$ within $T_\mu = 5$ s. Figure 9 shows the trajectories of v_i with asymmetric constraints, which confirms that the scaled relative velocities are confined within the prescribed region. As a result, the UAV follows the target at the desired relative position $l_d = [2, 0, 0]^{\mathrm{T}}$ m within the prescribed time $T_\gamma = 15$ s.

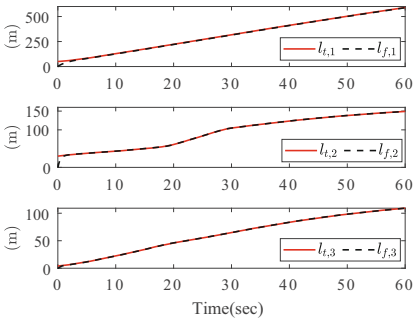

Figure 4 Trajectories of tracker and target in two-dimensional plane

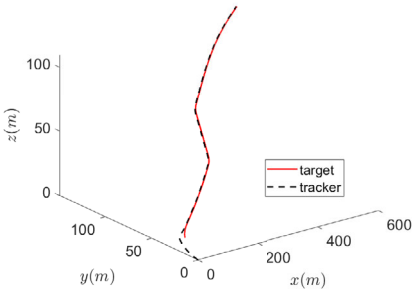

Figure 5 Trajectories of tracker and target in a three-dimensional plane

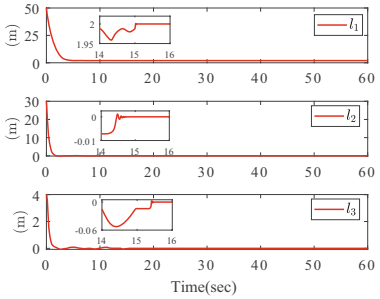

Figure 6 Relative distances between target and tracker

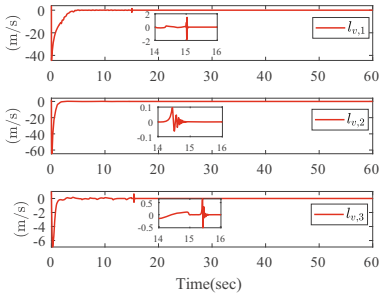

Figure 7 Relative velocities between target and tracker

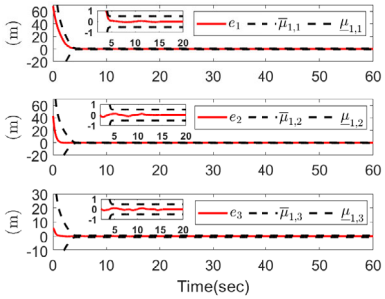

Figure 8 Tracking performance of scaled distance errors

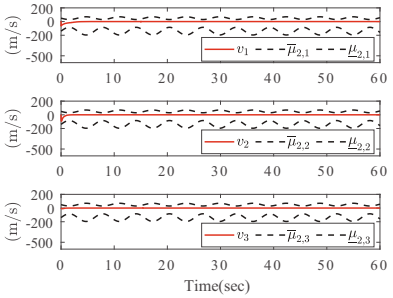

Figure 9 The scaled relative velocities under constraints

The comparative simulations are performed to prove the performance of the proposed control scheme in this paper.

Case 1 The proposed performance function is compared with the traditional performance function in [24], which is set to be $h_{1,i} = 97\exp(-0.01t) + 0.5$ and $-h_{1,i} < e_i < h_{1,i}$ for any time. The trajectories of e_i under different performance functions are shown in Figure 10. From Figure 10, the performance functions guarantee that the scaled distance error e_i converges to $[-0.5, 0.5]$. Compared to the result of [24], the performance function (11) has a faster convergence rate, which guarantees that e_i converges within predefined bounds at time $T_\mu = 5$ s.

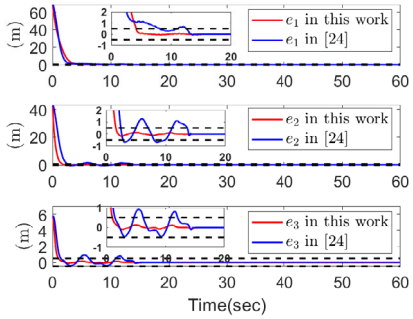

Figure 10 Comparative results of tracking performance under the proposed PPF and the conventional PPF in [24]

Case 2 In order to make a fair comparison between the designed controller and the fixed-time controller in [45], the other settings are the same except for the controller. With the same initial states, the trajectories of the relative distances and velocities under two controllers are depicted in Figures 11 and 12. Compared to the fixed-time controller in [45], the designed controller implements the characteristics of PPTS without oscillation and prescribed performance convergence.

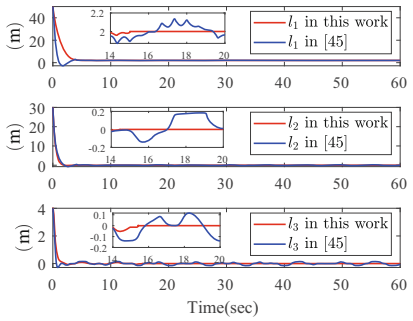

Figure 11 Comparative results of relative distances under the designed controller and the fixed-time controller in [45]

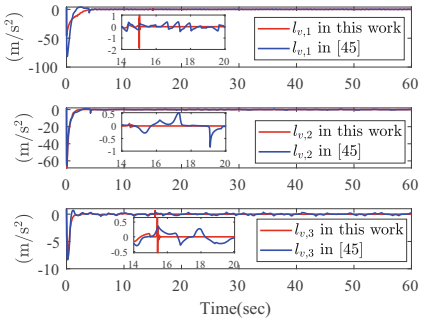

Figure 12 Comparative results of relative velocities under the designed controller and the fixed-time controller in [45]

6 Conclusions

This paper proposed a vision-based adaptive prescribed-time control strategy to guarantee the prescribed transient behavior and steady-state performance for uncooperative target tracking of UAV. A prescribed performance function with an unlimited initial value was constructed to ensure the prescribed-time tracking with the prescribed transient response. Based on the time-varying nonlinear transformation, the problems of performance constraint and scaled relative velocity constraint were transformed into a stability problem for the unconstrained system. Then, an adaptive prescribed-time controller guarantees that all states of the unconstrained system were bounded. In the future, we will focus on extending the work to the case of multiple UAVs.

Conflict of Interest

LI Hongyi is an editorial board member for Journal of Systems Science & Complexity and was not involved in the editorial review or the decision to publish this article. All authors declare that there are no competing interests.

References

[1] Ren W and Beard R W, Trajectory tracking for unmanned air vehicles with velocity and heading rate constraints, *IEEE Transactions on Control Systems Technology*, 2004, **12**(5): 706–716.

[2] Wang Y, Wang X, Zhao S, et al., Vector field based sliding mode control of curved path following for miniature unmanned aerial vehicles in winds, *Journal of Systems Science & Complexity*, 2018, **31**(1): 302–324.

[3] Ren H R, Ma H, Li H Y, et al., Adaptive fixed-time control of nonlinear MASs with actuator faults, *IEEE/CAA Journal of Automatica Sinica*, 2023, **10**(5): 1252–1262.

[4] Zheng X H, Li H Y, Ahn C K, et al., Observer-based finite-time consensus control for multiagent systems with nonlinear faults, *Information Sciences*, 2023, **621**: 183–199.

[5] Nocerino A, Opromolla R, Fasano G, et al., Lidar-based multi-step approach for relative state and inertia parameters determination of an uncooperative target, *Acta Astronautica*, 2021, **181**: 662–678.

[6] Stepanyan V and Hovakimyan N, Visual tracking of a maneuvering target, *Journal of Guidance, Control, and Dynamics*, 2008, **31**(1): 66–80.

[7] Zheng W, Zhou F, and Wang Z F, Robust and accurate monocular visual navigation combining IMU for a quadrotor, *IEEE/CAA Journal of Automatica Sinica*, 2015, **2**(1): 33–44.

[8] Liang J C, Chen Y J, Wu Y N, et al., Adaptive prescribed performance control of unmanned aerial manipulator with disturbances, *IEEE Transactions on Automation Science and Engineering*, 2023, **20**: 1804–1814.

[9] Chen G D, Liu Y, Yao D Y, et al., Event-triggered tracking control of nonlinear systems under sparse attacks and its application to rigid aircraft, *IEEE Transactions on Aerospace and Electronic Systems*, 2023, **59**(4): 4640–4650.

[10] Liu Y, Chi R H, Li H Y, et al., HiTL-based adaptive fuzzy tracking control of MASs: A distributed fixed-time strategy, *Science China Technological Sciences*, 2023, **66**: 2907–2916.

[11] Gao H J, An H, Lin W Y, et al., Trajectory tracking of variable centroid objects based on fusion of vision and force perception, *IEEE Transactions on Cybernetics*, 2023, **53**(12): 7957–7965.

[12] Zhang L L, Deng F, Chen J, et al., Vision-based target three-dimensional geolocation using unmanned aerial vehicles, *IEEE Transactions on Industrial Electronics*, 2018, **65**(10): 8052–8061.

[13] Lai N B, Chen Y J, Liang J C, et al., Image dynamics-based visual servo control for unmanned aerial manipulatorl with a virtual camera, *IEEE-ASME Transactions on Mechatronics*, 2022, **27**(6): 5264–5274.

[14] Zhang J, Wu Y, Liu W, et al., Novel approach to position and orientation estimation in vision-based UAV navigation, *IEEE Transactions on Aerospace and Electronic Systems*, 2010, **46**(2): 687–700.

[15] Jabbari A H and Yoon J, Robust image-based control of the quadrotor unmanned aerial vehicle, *Nonlinear Dynamics*, 2016, **85**(3): 2035–2048.

[16] Segal S, Carmi A, and Gurfil P, Stereovision-based estimation of relative dynamics between noncooperative satellites: Theory and experiments, *IEEE Transactions on Control Systems Technology*, 2013, **22**(2): 568–584.

[17] Yu Z Q, Liu Z X, Zhang Y M, et al., Distributed finite-time fault-tolerant containment control for multiple unmanned aerial vehicles, *IEEE Transactions on Neural Networks and Learning Systems*, 2019, **31**(6): 2077–2091.

[18] Sun P, Zhu B, Zuo Z Y, et al., Vision-based finite-time uncooperative target tracking for UAV subject to actuator saturation, *Automatica*, 2021, **130**: 109708.

[19] Zuo Z Y, Han Q L, Ning B D, et al., An overview of recent advances in fixed-time cooperative control of multiagent systems, *IEEE Transactions on Industrial Informatics*, 2018, **14**(6): 2322–2334.

[20] Jiménez-Rodríguez E, Muñoz-Vázquez A J, Sánchez-Torres J D, et al., A Lyapunov-like characterization of predefined-time stability, *IEEE Transactions on Automatic Control*, 2020, **65**(11): 4922–4927.

[21] Song Y D, Wang Y J, Holloway J, et al., Time-varying feedback for regulation of normal-form nonlinear systems in prescribed finite time, *Automatica*, 2017, **83**: 243–251.

[22] Becerra H M, Vázquez C R, Arechavaleta G, et al., Predefined-time convergence control for high-order integrator systems using time base generators, *IEEE Transactions on Control Systems Technology*, 2017, **26**(5): 1866–1873.

[23] Shao K and Zheng J C, Predefined-time sliding mode control with prescribed convergent region, *IEEE/CAA Journal of Automatica Sinica*, 2022, **9**(5): 934–936.

[24] Bechlioulis C P and Rovithakis G A, Robust adaptive control of feedback linearizable MIMO nonlinear systems with prescribed performance, *IEEE Transactions on Automatic Control*, 2008, **53**(9): 2090–2099.

[25] Xin B, Cheng S, Wang Q, et al., Fixed-time prescribed performance consensus control for multiagent systems with non-affine faults, *IEEE Transactions on Fuzzy Systems*, 2023, **31**(10): 3433–3446.

[26] Zheng X H, Ma H, Yao D Y, et al., Neural-based predefined-time distributed optimization of high-order nonlinear multiagent systems, *IEEE Transactions on Artificial Intelligence*, 2023, DOI: 10.1109/TAI.2023.3343684.

[27] Li Z, Zhang Y, and Zhang R, Prescribed error performance control for second-order fully actuated systems, *Journal of Systems Science & Complexity*, 2022, **35**(2): 660–669.

[28] Zhang L L, Che W W, Chen B, et al., Adaptive fuzzy output-feedback consensus tracking control of nonlinear multiagent systems in prescribed performance, *IEEE Transactions on Cybernetics*, 2022, **53**(3): 1932–1943.

[29] Ma H, Zhou Q, Li H, et al., Adaptive prescribed performance control of a flexible-joint robotic manipulator with dynamic uncertainties, *IEEE Transactions on Cybernetics*, 2021, **52**(12): 12905–12915.

[30] Zhang F K, Wu W M, and Wang C, Pattern-based learning and control of nonlinear pure-feedback systems with prescribed performance, *Science China Information Sciences*, 2023, **66**(1): 112202.

[31] Berger T, Le H H, and Reis T, Funnel control for nonlinear systems with known strict relative degree, *Automatica*, 2018, **87**: 345–357.

[32] Li Y F, Park J H, Hua C C, et al., Global output feedback tracking control for switched nonlinear systems with deferred prescribed performance, *Journal of the Franklin Institute*, 2021, **358**(3): 1743–1764.

[33] Zhao K, Song Y D, Chen C L P, et al., Adaptive asymptotic tracking with global performance for nonlinear systems with unknown control directions, *IEEE Transactions on Automatic Control*, 2021, **67**(3): 1566–1573.

[34] Wu J, He F R, Shen H, et al., Adaptive NN fixed-time fault-tolerant control for uncertain stochastic system with deferred output constraint via self-triggered mechanism, *IEEE Transactions on Cybernetics*, 2023, **53**(9): 5892–5903.

[35] Zhang H Y, Zhao X D, Wang H Q, et al., Adaptive tracking control for output-constrained switched MIMO pure-feedback nonlinear systems with input saturation, *Journal of Systems Science & Complexity*, 2023, **36**(3): 960–984.

[36] He H F, Qi W H, Yan H C, et al., Adaptive fuzzy resilient control for switched systems with state constraints under deception attacks, *Information Sciences*, 2023, **621**: 596–610.

[37] Ma H, Ren H R, Zhou Q, et al., Observer-based neural control of n-link flexible-joint robots, *IEEE Transactions on Neural Networks and Learning Systems*, 2022, DOI: 10.1109/TNNLS.2022.3203074.

[38] Niu B, Wang X A, Wang X M, et al., Adaptive Barrier-Lyapunov-functions based control scheme of nonlinear pure-feedback systems with full state constraints and asymptotic tracking performance, *Journal of Systems Science & Complexity*, 2024, **37**(3): 965–984.

[39] Liu L, Gao T T, Liu Y J, et al., Time-varying IBLFs-based adaptive control of uncertain nonlinear systems with full state constraints, *Automatica*, 2021, **129**: 109595.

[40] Yu J P, Zhao L, Yu H S, et al., Barrier Lyapunov functions-based command filtered output feedback control for full-state constrained nonlinear systems, *Automatica*, 2019, **105**: 71–79.

[41] Zhao K, Song Y D, and Zhang Z R, Tracking control of MIMO nonlinear systems under full state constraints: A single-parameter adaptation approach free from feasibility conditions, *Automatica*, 2019, **107**: 52–60.

[42] Guo C, Xie X J, and Hou Z G, Removing feasibility conditions on adaptive neural tracking control of nonlinear time-delay systems with time-varying powers, input, and full-state constraints, *IEEE Transactions on Cybernetics*, 2020, **52**(4): 2553–2564.

[43] Shi X C, Xu S Y, Jia X L, et al., Adaptive neural control of state-constrained MIMO nonlinear systems with unmodeled dynamics, *Nonlinear Dynamics*, 2022, **108**: 4005–4020.

[44] Huang Y and Jia Y M, Adaptive fixed-time six-DOF tracking control for noncooperative spacecraft fly-around mission, *IEEE Transactions on Control Systems Technology*, 2018, **27**(4): 1796–1804.

[45] She X H, Li X M, Yao D Y, et al., Vision-based adaptive fixed-time uncooperative target tracking for QUAV with unknown disturbances, *Journal of the Franklin Institute*, 2023, **360**(16): 12394–12414.

[46] Pan Y N, Ji W Y, Lam H K, et al., An improved predefined-time adaptive neural control approach for nonlinear multiagent systems, *IEEE Transactions on Automation Science and Engineering*, 2023, DOI: 10.1109/TASE.2023.3324397.

[47] Xiong J J and Zheng E H, Position and attitude tracking control for a quadrotor UAV, *ISA Transactions*, 2014, **53**(3): 725–731.

[48] Yao D Y, Li H Y, and Shi Y, Adaptive event-triggered sliding mode control for consensus tracking of nonlinear multi-agent systems with unknown perturbations, *IEEE Transactions on Cybernetics*, 2023, **53**(4): 2672–2684.

[49] Wang Z W, Liang B, Sun Y C, et al., Adaptive fault-tolerant prescribed-time control for teleoperation systems with position error constraints, *IEEE Transactions on Industrial Informatics*, 2019, **16**(7): 4889–4899.

[50] Sun J Y, Zhang H G, Wang Y C, et al., Fault-tolerant control for stochastic switched IT2 fuzzy uncertain time-delayed nonlinear systems, *IEEE Transactions on Cybernetics*, 2020, **52**(2): 1335–1346.